Chaotic scattering from hydrogen atoms in a circularly polarized laser field

Elias Okon, William Parker, Will Chism, and Linda E. Reichl
Center for Studies in Statistical Mechanics and Complex Systems, The University of Texas at Austin, Austin, Texas 78712
(Received 31 May 2002; published 15 November 2002)

We investigate the classical dynamics of a hydrogen atom in a circularly polarized laser beam with finite radius. The spatial cutoff for the laser field allows us to use scattering processes to examine the laser-atom dynamics. We find that for certain field parameters, the delay times, the angular momentum, and the distance of closest approach of the scattered electron exhibit fractal behavior. This fractal behavior is a signature of chaos in the dynamics of the atom-field system.

DOI: 10.1103/PhysRevA.66.053406 PACS number(s): 42.50.Hz, 32.80.Rm, 03.65.Nk

I. INTRODUCTION

The advent of high-energy lasers has allowed exploration of the dynamics of the laser-atom interaction in parameter regimes where the nonlinear character of the interaction dominates the dynamics. One of the most interesting developments is the stabilization of the atoms in high-energy laser fields. For the case of linearly polarized laser fields, stabilization has been predicted theoretically [1–5] and has been observed experimentally [6,7]. The origin of this stabilization appears to be phase-space structures induced by the nonlinear laser-field interaction.

Numerical studies [8–15] have shown that stabilization should also occur for atoms interacting with circularly polarized (CP) laser fields, although the underlying dynamics is much more complicated. Poincaré surfaces of section of the classical phase space show a very complex mixture of chaos and nonlinear resonance structures [11–14]. For hydrogen atoms, interacting with CP laser fields, stabilization appears to be caused by these complex structures which result from the interaction between the external field and the nonlinear atomic forces [13]. All work done to date on these systems assumes that the laser field extends spatially to infinity.

In this paper, we consider a more realistic spatial dependence for the laser field. We introduce a cutoff on the width of the laser beam. This then allows us to divide the configuration space into a reaction region interior to the beam, and an asymptotic scattering region exterior to the beam. The dynamics inside the reaction region is nonintegrable and the dynamics in the asymptotic region is integrable. With this more realistic picture of the geometry of the laser beam, we can probe the atom-laser dynamics using techniques of scattering theory, and we can ask different questions than those of previous studies. For example, in Refs. [11,12], the dynamics of the initially bound electron is studied as the laser pulse is turned on, and it is found that the ability of the electron to ionize is strongly determined by the position of the electron in the complex phase-space structures mentioned above. By using scattering theory, we can ask the complimentary question: for what initial conditions can an incident electron be captured for a long period of time? As we will see, the cutoff does not significantly affect the important electron-proton dynamics, so the scattered electron provides a systematic probe of the dynamics in the reaction region.

We begin in Sec. II by developing the classical model used to describe the electron-proton system in the presence of a circularly polarized laser beam with finite width. In Sec. III, we discuss the dynamics outside the influence of the laser beam. In Sec. IV, we look at the effect of the resonance structures and chaos in the reaction region on scattering properties of the electron. And finally, in Sec. V, we make some concluding remarks.

II. TWO-DIMENSIONAL CLASSICAL MODEL

We investigate the motion of the electron in a hydrogen atom (in the limit of an infinitely massive nucleus) driven by a CP laser field which has a finite width. The beam may consist of two linearly polarized laser beams superimposed, so that their Poynting vectors lie along the z axis, and their electric fields are polarized along the x axis and y axis, respectively. Outside some radius r (in the x-y plane), the electric field drops to zero. A realistic model for this cutoff is a Gaussian function of the radial distance r along with a parameter c that determines the rate of decay of the field strength. We restrict our model to the two-dimensional plane of polarization of the laser (the x-y plane). This simplification should capture the most important features of the dynamics, i.e., ionization or appearance of stable orbits which are expected to occur in that plane. In polar coordinates $(p_r, r, p_\theta, \theta)$ and in atomic units (a.u.), the planar Hamiltonian is given by

$$H = \frac{1}{2}\left(p_r^2 + \frac{p_\theta^2}{r^2}\right) - \frac{1}{\sqrt{\alpha^2 + r^2}} + F r e^{-cr^2} \cos(\theta - \omega t), \tag{1}$$

where F is the field strength, ω is the driving frequency, and α is a smoothing parameter. We set $\alpha = 0.8$ a.u., so the ionization potential is the same as that of hydrogen [10]. A suitable value for the cutoff parameter c is determined by experimentally obtainable sizes of focused laser beam spots. The size of the smallest possible laser beam spot is determined by the diffraction limit, and cannot be smaller than the wavelength of the laser. For visible light, (which is the one employed for the calculations throughout this paper) the parameter c must be in the order of 10^{-8} a.u. or smaller. However, because of computational considerations, we used $c = 10^{-5}$ a.u. This value of c is large enough to permit practi-

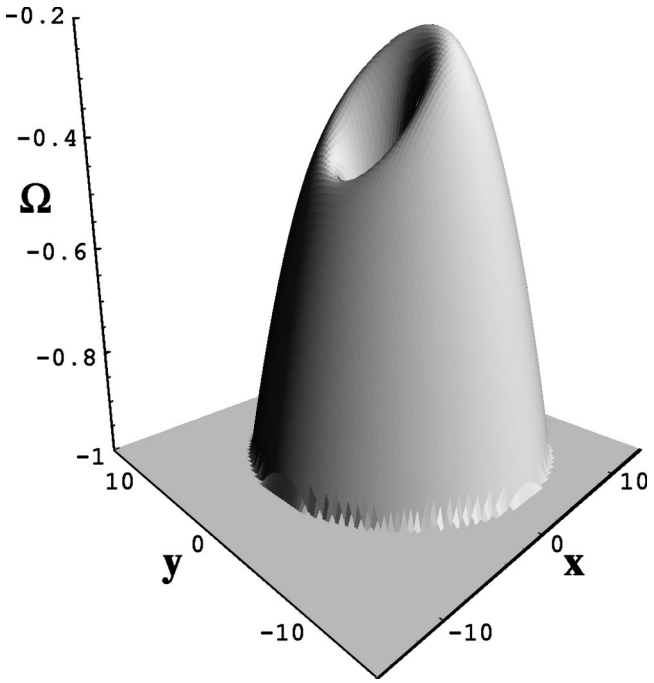

FIG. 1. Zero-velocity surface for $F=0.031\,935$ a.u., $\omega=0.114$ a.u., and $c=10^{-5}$ a.u.

cal calculations but small enough to retain most of the interesting structures in the system.

The time dependence of the Hamiltonian can be eliminated by performing a time-dependent canonical transformation, with generating function

$$F(p_\theta,\phi,p_r,\rho,t)=-p_\theta(\phi+\omega t)-p_r\rho \tag{2}$$

relating lab coordinates (p_r,r,p_θ,θ) to a coordinate frame $(P_\rho,\rho,P_\phi,\phi)$ that rotates with the electric field at a constant angular velocity ω. This leads to the Hamiltonian

$$H=\frac{1}{2}\left(P_\rho^2+\frac{P_\phi^2}{\rho^2}\right)-\frac{1}{\sqrt{\alpha^2+\rho^2}}+F\rho\ e^{-c\rho^2}\cos(\phi)-P_\phi\omega$$
$$=\Omega, \tag{3}$$

where the quasienergy Ω is a conserved energy in this rotating frame. If we introduce Cartesian coordinates in the rotating frame, $[x=\rho\cos(\phi), y=\rho\sin(\phi)]$, the electric field always lies along the x axis. Note that the Hamiltonian depends on ϕ, so the angular momentum P_ϕ is not conserved. In the subsequent discussion, we choose (unless otherwise stated) $\omega=0.114$ a.u., which corresponds to 400 nm laser excitation, and $F=0.319\,35$ a.u. ($I=3.58\times10^{13}\,\mathrm{W/cm^2}$) which is a "moderate" intensity associated with stabilization seen in numerical studies.

In the rotating frame, noninertial forces appear in the system, and lead to a mixing of position and momentum coordinates. This precludes the construction of a potential-energy surface in the usual sense. However, as shown in Refs. [11,12], it is possible to construct a zero-velocity surface (ZVS), which separates physical from unphysical regions of the phase space. If we recast the Hamiltonian in terms of the

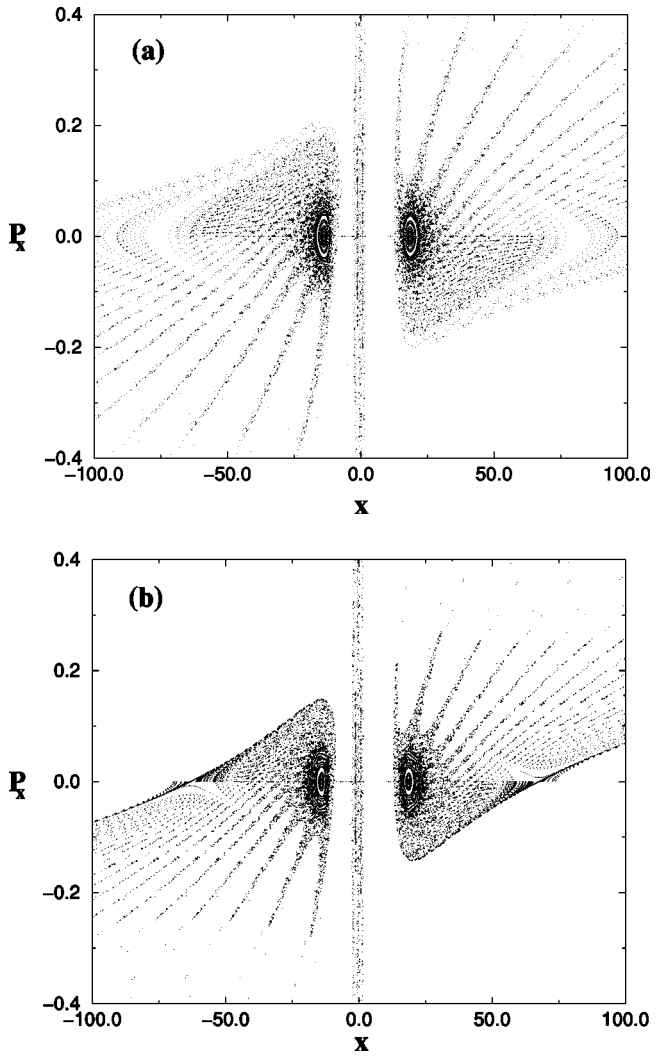

FIG. 2. Poincaré SOS at $\Omega=-0.451$ a.u. for (a) $c=0$ and (b) $c=10^{-5}$ a.u.

velocities $\dot\rho=P_\rho$ and $\dot\phi=P_\phi/\rho^2-\omega$, and then set $\dot\rho=0$ and $\dot\phi=0$, we obtain the equation for the ZVS,

$$\Omega_{\mathrm{ZVS}}=-\frac{1}{\sqrt{\alpha^2+\rho^2}}-\frac{1}{2}\omega^2\rho^2+F\rho\ e^{-c\rho^2}\cos(\phi). \tag{4}$$

The first two terms on the right-hand side of Eq. (4) result from the atomic force and centrifugal force, respectively, and have no angular dependence. They form a Coulomb well at small ρ and a quadratic falloff at large ρ. The angle-dependent term, due to the laser field, breaks the rotational symmetry. Just as was found in Refs. [11,12] for the case $c=0$, the ZVS can be depicted as a volcano with a confined "caldera" region (see Fig. 1). The ZVS helps to identify exclusion regions in phase space because a particle with nonzero velocity cannot intersect the ZVS.

The ZVS possesses two critical points, denoted by x_+ and x_-, that lie along the x axis on opposite sides of the proton and have quasienergies, $\Omega_+=\Omega_{zvs}(x_+)$ and $\Omega_-=\Omega_{zvs}(x_-)$, respectively. For any nonzero field, Ω_+

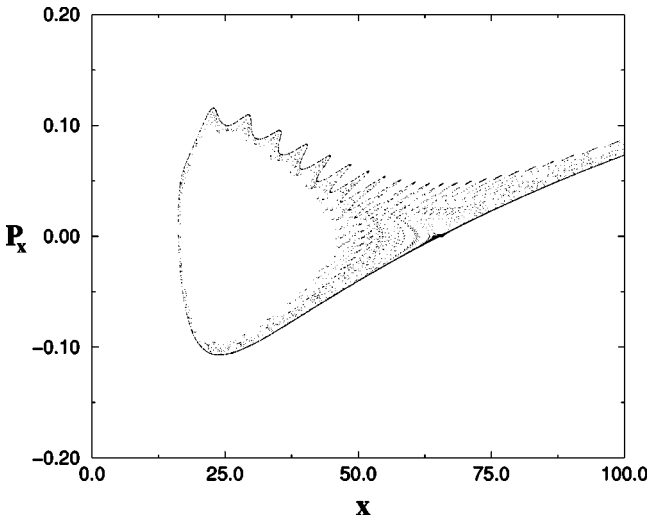

FIG. 3. A SOS in the neighborhood of the hyperbolic fixed point induced by the spatial cutoff of the laser field. The initial conditions lie in the interval 64 a.u. $\leqslant P_\rho \leqslant 66$ a.u., with $\Omega=-0.50$ a.u. and $c=10^{-5}$ a.u.

$>\Omega_-$. Thus, the quasienergy Ω will fall in one of the three regions: (1) $\Omega<\Omega_-$, (2) $\Omega_-\leqslant\Omega\leqslant\Omega_+$, or (3) $\Omega_+<\Omega$. When $\omega=0.114$ a.u. and $F=0.031\,935$ a.u., we have $\Omega_+=-0.119\,76$ a.u. and $\Omega_-=-0.469\,86$ a.u. We will use these values in the remainder of this paper. If $\Omega<\Omega_-$, the interior region (inside the caldera) cannot be reached by an electron lying outside the ZVS (but still inside the reaction region). However, if $\Omega>\Omega_-$, then some orbits can travel between the exterior region and the caldera and visit the vicinity of the proton.

The system whose dynamics is given by Eq. (3) has two degrees of freedom. Therefore, it is possible to construct a Poincaré surface of section (SOS). We will plot the radial momentum P_ρ and radial coordinate ρ each time $\phi=0$ and $\phi=\pi\ (\mathrm{mod}\pi)$. This can be thought of as a plot of P_x vs x, each time $y=0$ regardless of the sign of P_y. It is also useful to plot x vs y each time $P_\rho=0$ to obtain information about regions of configuration space accessible to the electron. In the surfaces of section shown in the subsequent sections, our initial conditions generally consist of a range of points with $P_\rho=0$ and $\phi=0$. The value of ρ is chosen randomly between 0 and a given ρ_{max} and the initial value of P_ϕ is determined by the quasienergy Ω.

Figure 2 shows a comparison of surfaces of section with and without the cutoff for $\Omega=-0.451$ a.u. We note that the SOS with $c=10^{-5}$ in Fig. 2(b), retains the significant nonlinear resonance structures and surrounding chaotic sea that can be seen in Fig. 2(a) and which has been seen by previous authors [11–14] for the case when the laser field extends to infinity. The large external resonance still exists [14] and the location of its central fixed point does not change significantly. However, the size of the external resonance and of the chaotic sea surrounding it is reduced. In addition, in Fig. 2(b) there is a pair of hyperbolic fixed points not present in the system without the cutoff. A plot with $\Omega=-0.50$ a.u. and initial conditions, 64 a.u. $\leqslant P_\rho \leqslant 66$ a.u., confined to the neighborhood of the "cutoff" induced hyperbolic point (see

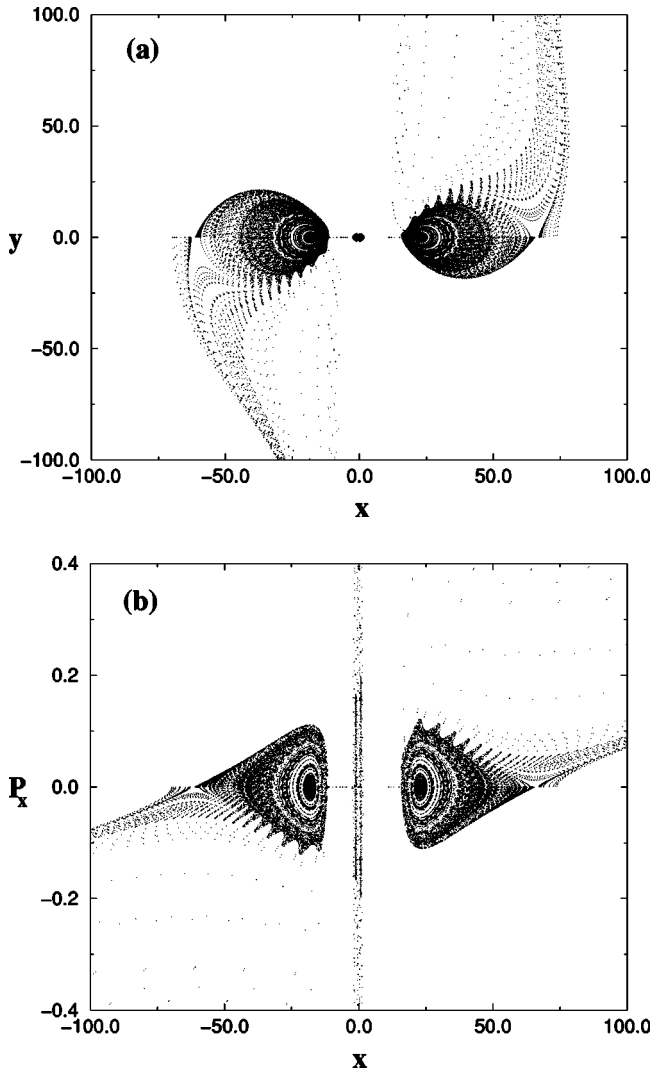

FIG. 4. All graphs in this figure correspond to $\Omega=-0.496$ a.u. and $c=10^{-5}$ a.u. (a) Surface of section, y vs x (in a.u.) for initial conditions $p_x=0$, -70 a.u. $\leqslant x \leqslant 70$ a.u. (b) Surface of section, p_x vs x (in a.u.) for the same initial conditions as in (a).

Fig. 3) shows clearly the contracting and expanding directions of the phase space in the neighborhood of the hyperbolic fixed point. By extending the initial conditions further out from the nucleus, but still along $\phi=0$, we found yet another pair of elliptic and hyperbolic points in each side of the nucleus.

III. ASYMPTOTIC SCATTERING REGION

When ρ is large enough so that the field term can be neglected, the Hamiltonian reduces to an asymptotic Hamiltonian H_{asym} given by

$$H_{asym}=\frac{1}{2}\left(P_\rho^2+\frac{P_\phi^2}{\rho^2}\right)-\frac{1}{\rho}-P_\phi\omega=\Omega. \tag{5}$$

This Hamiltonian is equivalent to that of the Kepler problem (particle in a central attractive inverse square-law force), as

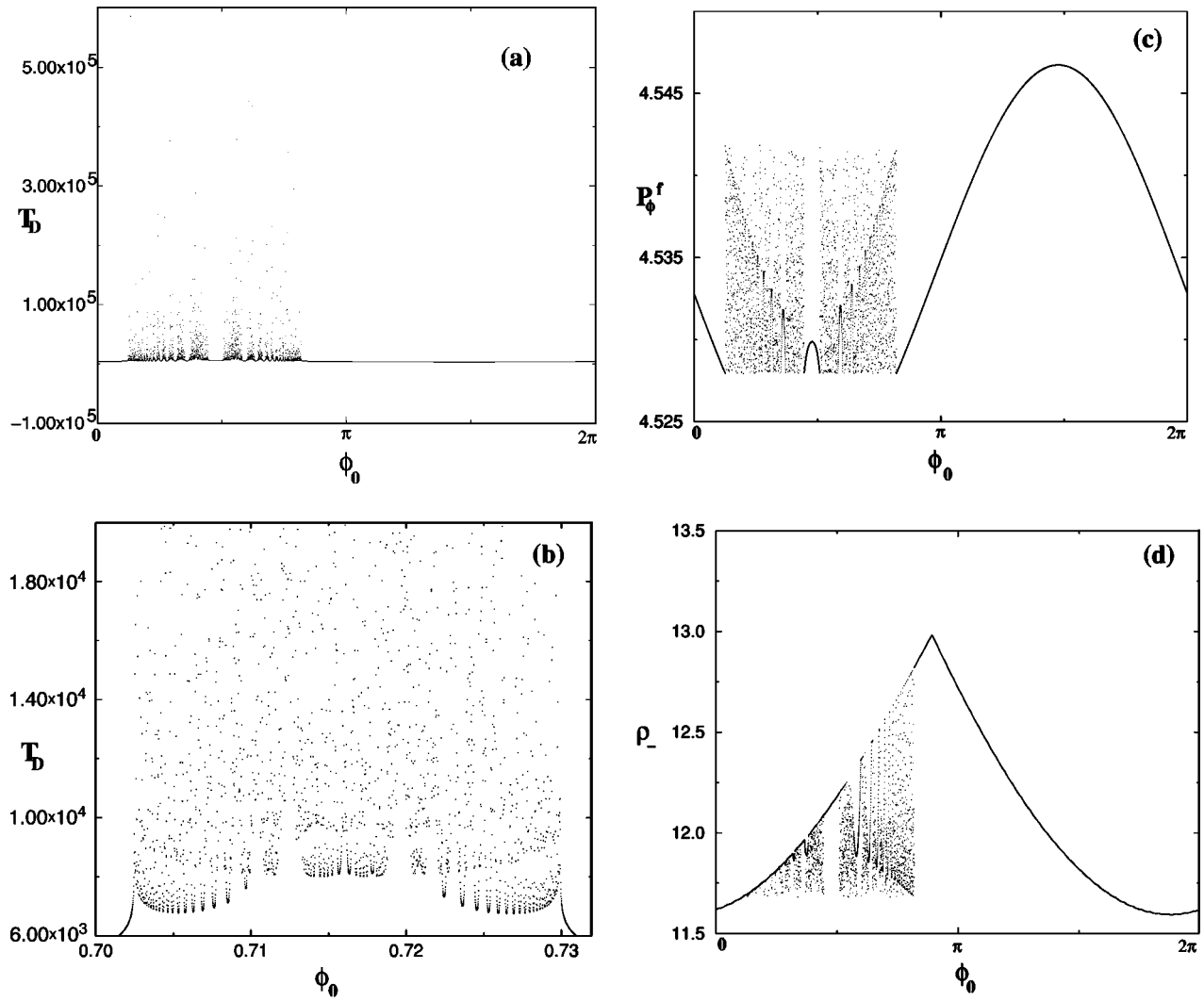

FIG. 5. Scattering data for $\Omega=-0.496$ a.u. and initial angular momentum $P_\phi^i=4.530\,653\,3$ a.u. (a) Delay time T_D (in a.u.) vs ϕ_0 for $0\leqslant\phi_0\leqslant 2\pi$. (b) T_D vs ϕ_0 for $0.702\leqslant\phi_0\leqslant 0.735$. (c) Final angular momentum P_ϕ^f (in a.u.) vs ϕ_0 for $0\leqslant\phi_0\leqslant 2\pi$. (d) Radius of closest approach ρ_- (in a.u.) vs ϕ_0 for $0\leqslant\phi_0\leqslant 2\pi$.

seen in a frame rotating with frequency ω. The equations of motion of this system can be integrated analytically yielding closed-form solutions to the orbits in the asymptotic region. The radial component of the motion in the rotating frame is identical to that of the nonrotating frame. However, in the rotating frame the actual trajectories cease to be conic sections due to Coriolis forces which are present in the rotating frame.

Let us consider the dynamics generated by the Hamiltonian H_{asym}. The orbits of H_{asym} can be specified uniquely in terms of three quantities: the two conserved quantities, Ω and P_ϕ (which are both conserved by H_{asym}); and by a third quantity ϕ_0, which is the initial angle of the orbit. The total energy of an orbit in the lab frame, $E=\Omega_{asym}+\omega P_\phi$, determines if that orbit is closed (bounded) or open (unbounded). If $E<0$, the motion is bounded. If $E>0$, the motion is unbounded and the trajectory comes in from infinity up to a point of closest approach, $\rho=\rho_-$, then returns to infinity. For $E>0$, the point of closest approach is $\rho_-=a(1-e)$, where $a=-1/2E$ and $e=\sqrt{1+2P_\phi^2E}$ is the eccentricity. The value of ρ_- is determined by the total energy E and the total angular momentum P_ϕ.

If we draw a circle of radius R centered at $(x=0, y=0)$, we can determine the time required for an orbit to traverse the interior of the circle after it first enters it at $\rho=R$. Let τ be the time to travel from $\rho=R$ to $\rho=\rho_-$. It is straightforward to solve the equation of motion and obtain an analytic expression for τ. We find

$$\tau=\sqrt{|a|}\{\sqrt{(R-\rho_-)(R+\rho_-)}+a\ln[\,2\sqrt{(R-\rho_-)(R+\rho_-)}+R-2a\,]-a\ln[\,2e|a|\,]\}. \tag{6}$$

Because of the symmetry of the orbit, the total time the orbit spends inside the circle is 2τ when $F=0$.

IV. FRACTAL BEHAVIOR IN THE SCATTERING PROCESS

We can now use the information about the dynamics when $F=0$ to probe the dynamics of the system when $F\neq 0$. The

following method is employed. For the case when $F \neq 0$, an electron with fixed Ω and P_ϕ and with a range of values for ϕ_0 is launched inwards from a point $(\rho = R, \phi = \phi_0)$. We choose R large enough so that it lies in the asymptotic region. The trajectory enters the circle at time $t = 0$, interacts with the the laser field and atomic forces, and after a finite time T_R, it leaves the circle. The functional dependence on ϕ_0 of the excursion time T_R, the angular momentum P_ϕ^f, and the distance of closest approach to the nucleus, ρ_-, are analyzed. Specifically we numerically generate plots of the delay time, $T_D = T_R - 2\tau$, the final angular momentum P_ϕ^f, and the distance of closest approach, ρ_-, as a function of ϕ_0. The delay time T_D is the actual time the particle spends inside the circle, minus the time 2τ calculated for the trajectory with the asymptotic Hamiltonian alone.

Below we explore the dynamics in the quasienergy regimes $\Omega < \Omega_-$ and $\Omega_- \leqslant \Omega \leqslant \Omega_+$. In subsequent plots, we choose the radius of the circle to be $R = 1500.0$ a.u., for which the laser-field term in the Hamiltonian can be safely neglected. The values of ϕ_0 are evenly distributed in the interval $[0, 2\pi]$ and 10 000 different values of ϕ_0 are chosen. Below we first consider the regime $\Omega < \Omega_-$, and then the regime $\Omega_- \leqslant \Omega \leqslant \Omega_+$.

A. The quasienergy regime $\Omega < \Omega_-$

We begin with quasienergies in the regime $\Omega < \Omega_-$, where the ZVS divides the phase space into two unconnected areas, the central caldera and the exterior region. For $\Omega = -0.496$ a.u., the SOS exhibits a large exterior resonance, as shown in Figs. 4(a) and 4(b). The initial conditions for both Figs. 4(a) and 4(b) include a line of points at $p_x = 0$ ranging from $x = -70$ a.u. to $x = 70$ a.u. Although both these plots show orbits in the interior and exterior regions, this only happens because some initial points span those two regions. There are no orbits that transit between these regions.

In Fig. 5, we show plots of the delay time T_D, the final angular momentum P_ϕ^f, and the radius of closest approach, ρ_-, for initial conditions, $\Omega = -0.496$ a.u., $P_\phi^i = 4.530\,653\,3$ a.u., and $0 \leqslant \phi_0 \leqslant 2\pi$. These plots show fractal behavior for initial angles in the interval $0.395 \leqslant \phi_0 \leqslant 2.575$. In Fig. 5(b), we focus on a small interval 0.70 a.u. $\leqslant \phi_0 \leqslant 0.735$ a.u. from the fractal segment in Fig. 5(a). The fractal behavior continues to repeat itself on smaller scales. In Fig. 5(c), we show the final angular momentum P_ϕ^f for initial angles in the interval $0 \leqslant \phi_0 \leqslant 2\pi$. This shows the same fractal behavior as the delay time. In Fig. 5(d), we show the radius of closest approach, ρ_-, for the range of initial conditions $0 \leqslant \phi_0 \leqslant 2\pi$. This also shows fractal behavior in the interval $0.395 \leqslant \phi_0 \leqslant 2.575$. Note that the electron never gets close to the proton.

As discussed in Refs. [16–18], fractal behavior in the scattering properties is an indicator that the electron has traversed a network of heteroclinic tangles (chaotic structures) as it passes through the reaction region. To see this more clearly, in Fig. 6, we examine some typical orbits from the fractal region in Fig. 5. Figure 6(a) shows a surface of section of p_x vs x for a set of orbits with initial angular momentum $P_\phi^i = 4.530\,653\,3$ a.u. and initial angles in the interval $0.5 \leqslant \phi_0 \leqslant 1.0$. In the SOS, orbits are plotted for $\phi = 0$ and $\phi = \pi$. These orbits clearly lie along the contracting and expanding manifolds associated with the exterior resonance. Figure 6(b) shows the path in the x-y plane (not a SOS) of a single orbit with initial angular momentum $P_\phi^i = 4.530\,653\,3$ a.u. and initial angle $\phi_0 = 1.294\,525\,6$. It is clearly trapped in the exterior part of the reaction region for a long period of time. Figure 6(c) shows the variation of the angular momentum of the orbits in Fig. 6(a) as a function of time.

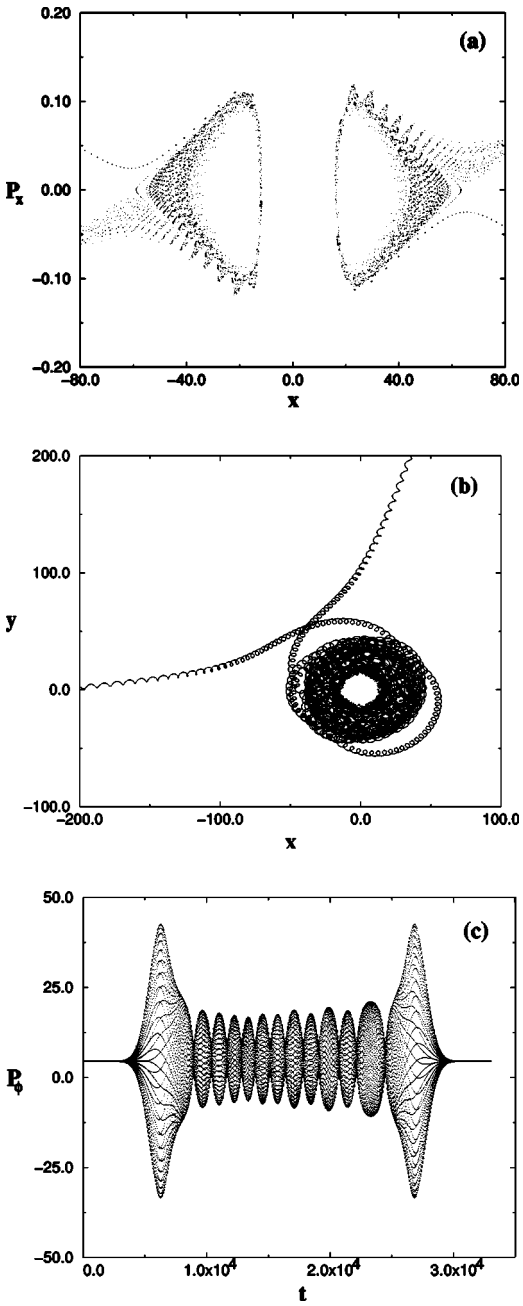

FIG. 6. Some typical orbits from the fractal regime for $\Omega = -0.496$ a.u. and $P_\phi^i = 4.530\,653\,3$ a.u. (a) Surface of section of p_x vs x (in a.u.) for $0.5 \leqslant \phi_0 \leqslant 1.0$. (b) A single trajectory in the x-y plane for $P_\phi^i = 4.530\,653\,3$ a.u. and $\phi_0 = 1.294\,525\,6$. (c) P_ϕ vs time t (in a.u.) for trajectories in the interval $0.5 \leqslant \phi_0 \leqslant 1.0$.

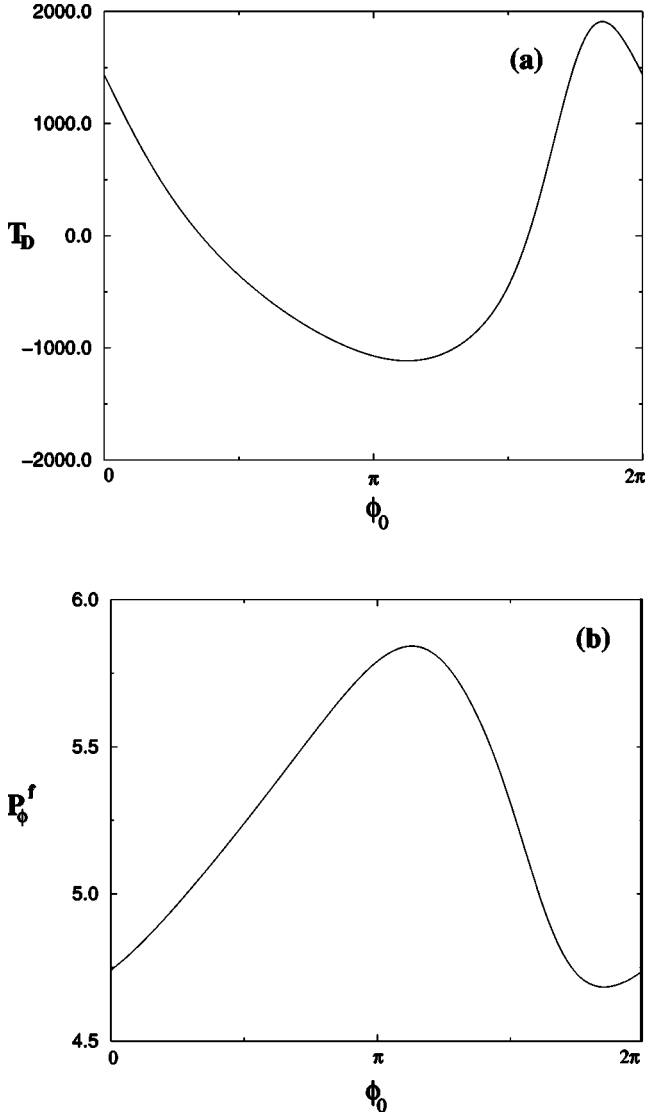

FIG. 7. Scattering data for $\Omega=-0.496$ a.u. and $P_\phi^i=5.0$ a.u. (a) Delay time T_D (in a.u.) vs ϕ_0 for $0\leqslant\phi_0\leqslant 2\pi$. (b) Final angular momentum P_ϕ^f (in a.u.) vs ϕ_0 for $0\leqslant\phi_0\leqslant 2\pi$.

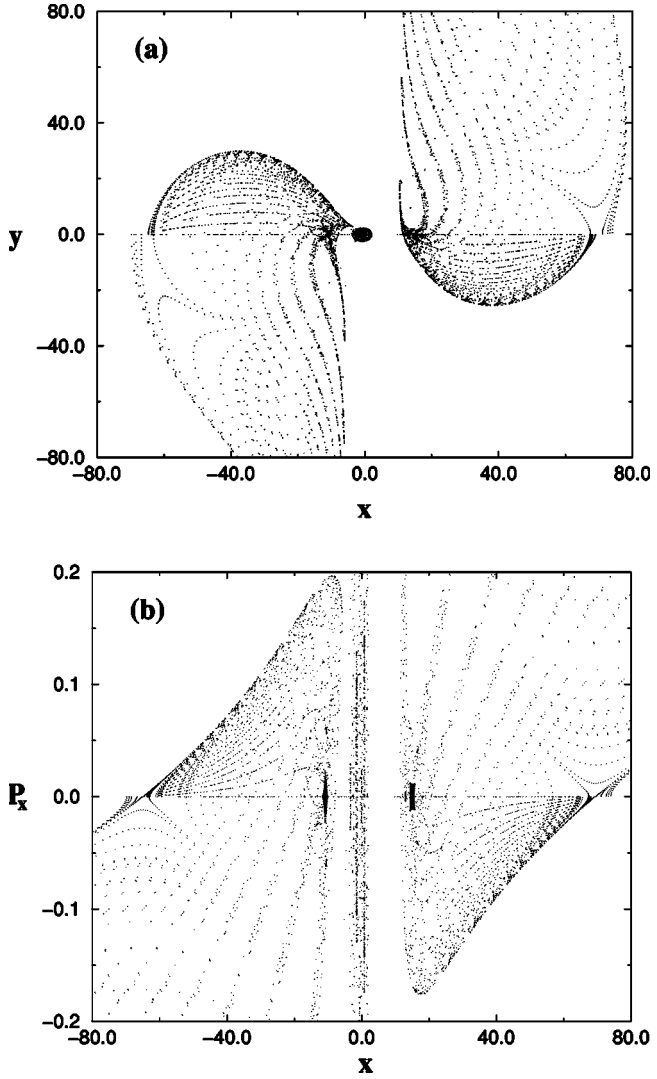

FIG. 8. Graphs correspond to $\Omega=-0.406$ a.u. and $c=10^{-5}$ a.u. (a) Surface of section y vs x for initial conditions $p_x=0$ and -70 a.u. $\leqslant x\leqslant 70$ a.u. (b) Surface of section p_x vs x (in a.u.) for the same initial conditions as in (a).

Not all initial conditions allow the trajectory to enter the exterior resonance region. In Figs. 7(a) and 7(b), we show plots of the delay time T_D, and the asymptotic angular momentum P_ϕ^f, respectively, as a function of ϕ_0 for $\Omega=-0.496$ a.u., $P_\phi^i=5.0$ a.u., and $0\leqslant\phi_0\leqslant 2\pi$. In both cases, we obtain simple smooth curves. Note that T_D has a large range of values, -1000 a.u. $\leqslant T_D\leqslant 1500$ a.u., and that large T_D values are associated with small values of P_ϕ^f. On the other hand, the negative values of T_D correspond to orbits that receive a large increase in the angular momentum P_ϕ, in the reaction region, and leave the reaction region much faster due to the presence of the laser field.

B. The quasienergy regime $\Omega_-\leqslant\Omega\leqslant\Omega_+$

Let us now consider the regime $\Omega_-\leqslant\Omega\leqslant\Omega_+$, in which the caldera and the exterior region are connected by a passageway. For some initial conditions, the electron can enter the caldera and come near the proton. In Fig. 8(a), we show a surface of section of x vs y for $\Omega=-0.406$ a.u. and plotted each time $p_x=0$. The initial condition includes a line of points, -70 a.u. $\leqslant x\leqslant 70$ a.u. In Fig. 8(b), we show a SOS of p_x vs x for the same initial conditions used in Fig. 8(a). We see that the exterior resonance is still intact but the area of the regular island is much smaller than in Figs. 4(a) and 4(b), and it has moved closer to the origin. Also, the area affected by the heteroclinic tangles has increased considerably. The inward shift of the location of the elliptic fixed point of the resonance with the increase of Ω causes more orbits to collide with the ZVS, leading to their eventual chaotic ionization.

In Figs. 9(a) and 9(c), we show plots of the delay time T_D and the final angular momentum P_ϕ^f, as a function of ϕ_0 in the interval $0\leqslant\phi_0\leqslant 2\pi$. All plots in Fig. 9 are for quasienergy $\Omega=-0.406$ a.u. and initial angular momentum $P_\phi^i=5.0$ a.u. We again see a range of fractal behavior in each

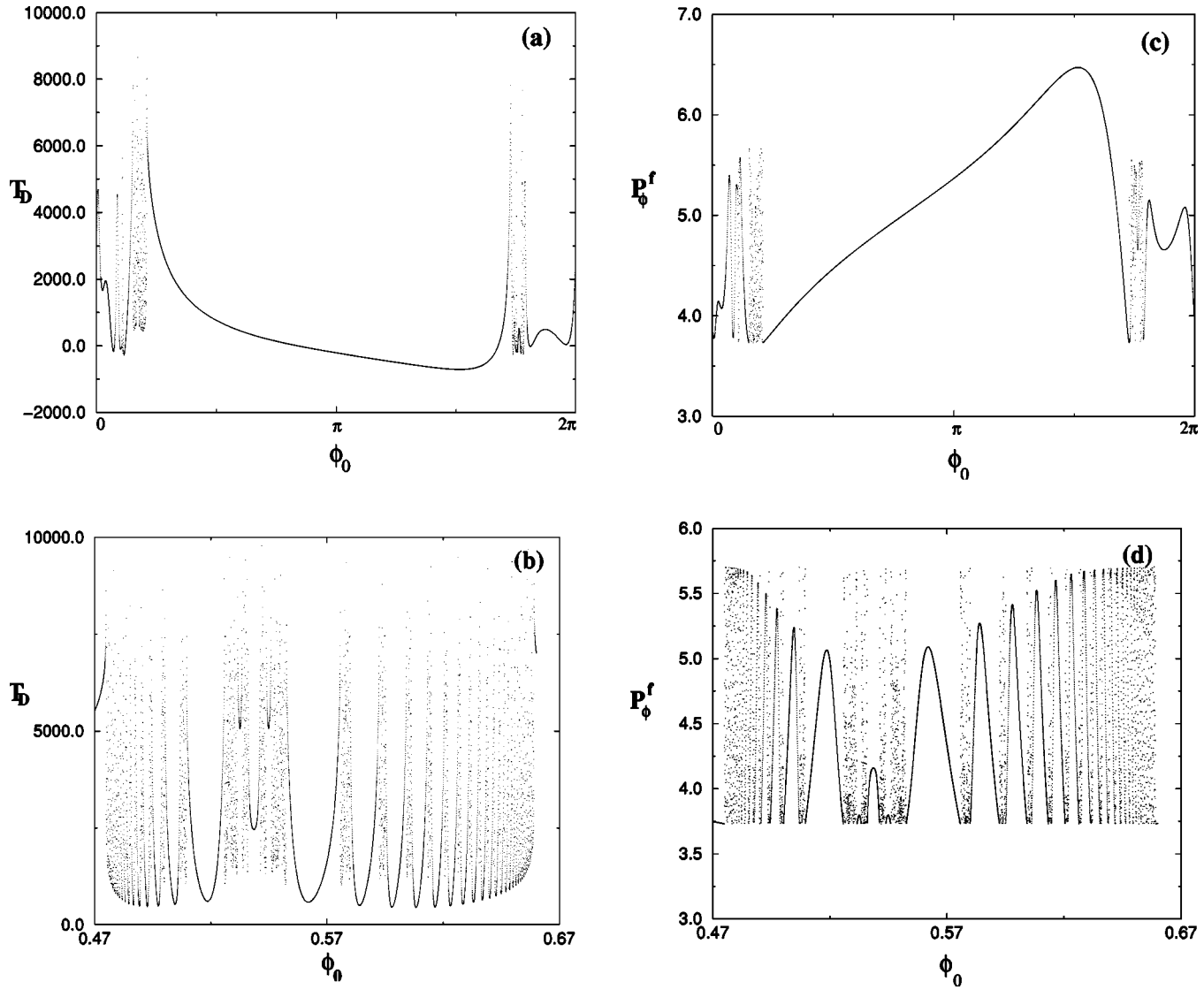

FIG. 9. Scattering data for $\Omega=-0.406$ a.u. and $P_\phi^i=5.0$ a.u. (a) Delay time T_D (in a.u.) vs ϕ_0 for $0\leqslant\phi_0\leqslant 2\pi$. (b) T_D (in a.u.) vs ϕ_0 for $0.47\leqslant\phi_0\leqslant 0.67$. (c) Final angular momentum P_ϕ^f (in a.u.) vs ϕ_0 for $0\leqslant\phi_0\leqslant 2\pi$. (d) P_ϕ^f (in a.u.) vs ϕ_0 for $0.47\leqslant\phi_0\leqslant 0.67$.

plot. In Fig. 9(a), we show the delay time T_D for the entire range of initial angles, $0\leqslant\phi_0\leqslant 2\pi$, and in Fig. 9(b) we focus on a small interval $0.47\leqslant\phi_0\leqslant 0.67$ and magnify the horizontal scale of one of the unresolved regions. We can see that the function is still not resolved. This clearly suggests a complex structure at even smaller scales, and we find that to be the case. In Figs. 9(c) and 9(d), we show plots for the angular momentum P_ϕ^f of the scattered electron for the same two ranges of the initial angle as shown in Figs. 9(a) and 9(b). The angular momentum of the scattered particle can take on a huge range of values after passing through the resonance region. For a small range of initial angles, the electron does enter the interior region and comes relatively close to the proton.

In order to confirm that the fractal behavior in the T_D plots is related to the chaotic structures in the phase space, it is useful to construct a SOS for the orbits that generate the fractal structures in Fig. 9. In Fig. 10(a) we show a SOS of p_x vs x for initial condidtions, $\Omega=-0.406$ a.u., $P_\phi^i=5.0$ a.u., and $0.47\leqslant\phi_0\leqslant 0.67$. Only those orbits with $\dot{y}>0$ are shown. These orbits get trapped for long time in the heteroclinic tangles associated with the exterior region and do not enter the caldera. In Fig. 10(b) we show a single orbit, with $P_\phi^i=5.0$ a.u. and $\phi_0=0.5$. This orbit does not enter the caldera, but does get delayed for a significant period of time in the reaction region. In Fig. 10(c), we show the angular momentum as a function of time for the orbits in Fig. 10(a). The angular momentum appears to decrease while the orbit is trapped in the exterior resonance region.

In Fig. 11(a), we show a single orbit which enters the caldera for the case $\Omega=-0.406$ a.u., taken from the fractal region with $P_\phi^i=5.0$ a.u. and $\phi_0=5.585\,68$ a.u. This orbit gets trapped for a long time inside the caldera. In Fig. 11(b), we show the angular momentum as a function of time for the same orbit as in Fig. 11(a). It is interesting that during the

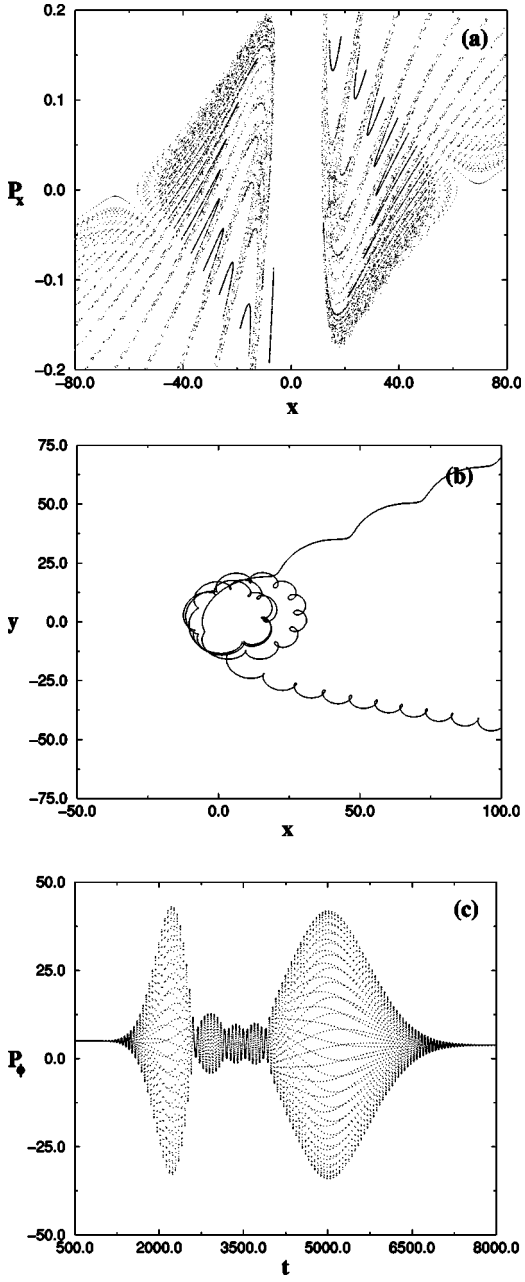

FIG. 10. Some typical orbits which get trapped in the exterior region for $\Omega=-0.406$ a.u. (a) p_x vs x (in a.u.) for $P^i_\phi=5.0$ a.u. and $0.47\leqslant\phi_0\leqslant0.67$. (b) x vs y (not a SOS) for a single orbit with $P^i_\phi=5.0$ a.u. and $\phi_0=0.55$. (c) P_ϕ vs time t for $P^i_\phi=5.0$ a.u. and $\phi_0=0.55$ (in a.u.).

time the orbit spends inside the caldera, it has a very low angular momentum as one might expect since the radius remains small.

V. CONCLUSIONS

We have examined the classical dynamics of an electron-proton system (the hydrogen atom when they are bound) which interacts with an intense circularly polarized laser beam of finite radius. We have explored dynamics of the system by launching electrons into the reaction region and

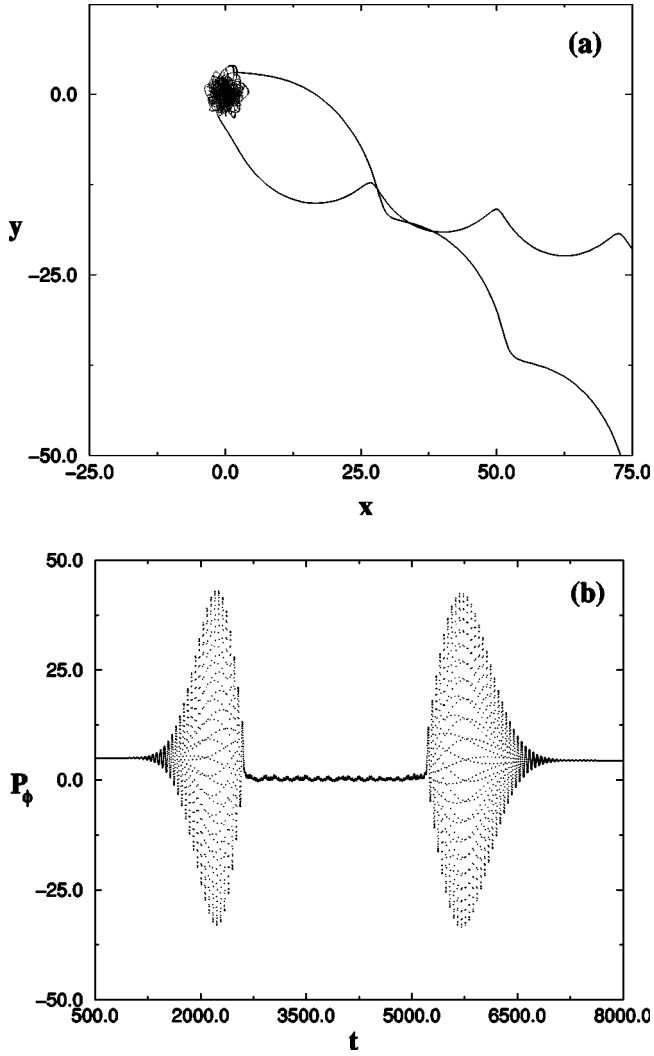

FIG. 11. A typical orbit from the fractal regime for $\Omega=-0.406$ a.u. and initial angular momentum $P^i_\phi=5.0$ a.u. (a) A single trajectory in the x-y plane (not a SOS) for $P^i_\phi=5.0$ a.u. and $\phi_0=5.585\,68$. (b) P_ϕ vs time t (in a.u.) for the same orbit as in (a).

plotting the delay time, the exiting angular momentum, and the distance of closest approach as a function of the incident angle. The dynamics has two distinct regimes depending on the value of the quasienergy of the incident particle. Below a certain cutoff value of the quasienergy, no initial condition will allow the incident electron to come close to the proton. Above that cutoff value quasienergy, a finite range (which grows with increasing value of quasienergy) can come arbitrarily close to the proton (this separation of regimes was also noted in Refs. [11–14]).

We have found that incident orbits can exhibit fractal behavior in their delay time, the exiting angular momentum, and the distance of closest approach as a function of the incident angle after they exit the reaction region. The appearance of fractal behavior in the scattering plots is closely related to the trapping of incoming orbits in the chaotic structures surrounding the stable islands in the phase space.

Using scattering theory to probe the electron-proton dynamics gives a systematic way of finding the chaotic regions

of the phase space and regions that can trap the electron for long periods. Use of scattering theory can also give some information about ionizing orbits, since for every incident orbit, there will be a time-reversed ionizing orbit. Our results show a strong directional dependence of initial states that can be delayed for long periods in the reaction region. It might be possible to observe this directional dependence in the scattering of electrons off a proton beam as it passes through a circularly polarized laser beam.

ACKNOWLEDGMENTS

The authors wish to thank the Welch Foundation, Grant No. F-1051, NSF Grant No. INT-9602971, and DOE Contract No. DE-FG03-94ER14405 for partial support of this work. We also thank the University of Texas at Austin High Performance Computing Center for use of their computer facilities, and we thank Christof Jung for very useful conversations.

[1] J.H. Eberly and K.C. Kulander, Science **262**, 1229 (1993).
[2] Q. Su and J.H. Eberly, J. Opt. Soc. Am. B **7**, 564 (1990).
[3] Q. Su, J.H. Eberly, and J. Javanainen, Phys. Rev. Lett. **64**, 862 (1990).
[4] R.V. Jensen and B. Sundaram, Phys. Rev. Lett. **65**, 1964 (1990).
[5] B. Sundaram and R.V. Jensen, Phys. Rev. A **47**, 1415 (1993).
[6] M.P. de Boer *et al.*, Phys. Rev. Lett. **71**, 3263 (1993); Phys. Rev. A **50**, 4085 (1994).
[7] N.J. Druten, R.C. Constantinescu, J.M. Schins, H. Nieuwenhuize, and H.G. Muller, Phys. Rev. A **55**, 622 (1997).
[8] J. Zakrzewski and D. Delande, J. Phys. B **28**, L667 (1995).
[9] M. Pont and M. Gavrila, Phys. Rev. Lett. **65**, 2362 (1990); M. Pont, Phys. Rev. A **40**, 5659 (1989).
[10] A. Patel, M. Protopapas, D.G. Lappas, and P.L. Knight, Phys. Rev. A **58**, R2652 (1998); A. Patel, N.J. Kylstra, and P.L. Knight, Opt. Express **4**, 496 (1999).
[11] A.F. Brunello, T. Uzer, and D. Farrelly, Phys. Rev. A **55**, 3730 (1997).
[12] D. Farrelly and T. Uzer, Phys. Rev. Lett. **74**, 1720 (1995).
[13] Will Chism, Dae-Il Choi, and L.E. Reichl, Phys. Rev. A **61**, 054702 (2000).
[14] W. Chism and L.E. Reichl, Phys. Rev. A **65**, 21404R (2002).
[15] Iwo Bialymicki-Birula, Maciej Kalinski, and J.H. Eberly, Phys. Rev. Lett. **73**, 1777 (1994).
[16] E. Ott and T. Tl, Chaos **3**, 417 (1993).
[17] E. Ott, *Chaos in Dynamical Systems* (Cambridge University Press, Cambridge, England, 1993).
[18] C. Jung and T.H. Seligman, Phys. Rep. **285**, 77 (1997).